

A robust broadband fat-suppressing phaser T_2 -preparation module for cardiac magnetic resonance imaging at 3T

Lionel Arn¹ | Ruud B. van Heeswijk¹  | Matthias Stuber^{1,2}  |
Jessica A. M. Bastiaansen¹  

¹Department of Diagnostic and Interventional Radiology, Lausanne University Hospital and University of Lausanne, Lausanne, Switzerland

²Center for Biomedical Imaging, Lausanne, Switzerland

Correspondence

Jessica A. M. Bastiaansen, Department of Diagnostic and Interventional Radiology, University Hospital Lausanne (CHUV), Rue de Bugnon 46, BH 08.074, 1011 Lausanne, Switzerland.

Email: jbastiaansen.mri@gmail.com

Funding information

The Swiss National Science Foundation (grant nos. PZ00P3_167871, PCEFP2_194296, 32003B_182615, 320030_173129, and 326030_150828), the Emma Muschamp Foundation, the Swiss Heart Foundation (grant nos. FF18054 and FF20136), and the Bourse Pro Femmes from the University of Lausanne

Purpose: Designing a new T_2 -preparation (T_2 -Prep) module to simultaneously provide robust fat suppression and efficient T_2 preparation without requiring an additional fat-suppression module for T_2 -weighted imaging at 3T.

Methods: The tip-down radiofrequency (RF) pulse of an adiabatic T_2 -Prep module was replaced by a custom-designed RF-excitation pulse that induces a phase difference between water and fat, resulting in a simultaneous T_2 preparation of water signals and the suppression of fat signals at the end of the module (a phaser adiabatic T_2 -Prep). Numerical simulations and in vitro and in vivo electrocardiogram (ECG)-triggered navigator-gated acquisitions of the human heart were performed. Blood, myocardium, and fat signal-to-noise ratios and right coronary artery vessel sharpness were compared against previously published adiabatic T_2 -Prep approaches.

Results: Numerical simulations predicted an increased fat-suppression bandwidth and decreased sensitivity to transmit magnetic field inhomogeneities using the proposed approach while preserving the water T_2 -Prep capabilities. This was confirmed by the tissue signals acquired in the phantom and the in vivo images, which show similar blood and myocardium signal-to-noise ratio, contrast-to-noise ratio, and significantly reduced fat signal-to-noise ratio compared with the other methods. As a result, the right coronary artery conspicuity was significantly increased.

Conclusion: A novel fat-suppressing T_2 -Prep method was developed and implemented that showed robust fat suppression and increased vessel sharpness compared with conventional techniques while preserving its T_2 -Prep capabilities.

KEYWORDS

3T magnetic resonance imaging (MRI), adiabatic, angiography, coronary, fat suppression, noncontrast, T_2 preparation

1 | INTRODUCTION

Noncontrast-enhanced pulse sequences often lack the required contrast to distinguish blood from the myocardium in cardiac MRI. T_2 -preparation (T_2 -Prep) modules¹ allow this

contrast to be increased by using the difference in T_2 relaxation times between these two tissue types.^{2,3} Such modules are also used for robust T_2 mapping of the myocardium and knee cartilage.^{4,6} In these applications, unwanted signal from fat can compromise the delineation and anatomical

visualization of the tissue of interest, such as cartilage,⁷ myocardium, or the coronary vessels,⁸ and thus decrease image quality. Unsuppressed fat signal may also lead to water-fat-signal cancellation and can accentuate artifacts.

To suppress an unwanted lipid signal, pulse sequences usually include additional fat signal-suppressing approaches, such as chemically selective saturation (CHESS),⁹ water-excitation,¹⁰⁻¹² or frequency-selective inversion RF pulses.^{13,14} Higher magnetic field strengths may complicate conventional fat-saturation and T₂-Prep techniques, which are sensitive to B₀ and B₁ field inhomogeneities. The use of adiabatic RF-excitation pulses addressed the sensitivity to B₁ inhomogeneities.¹⁵⁻¹⁸ By introducing a delay before the tip-up pulse of an adiabatic T₂-Prep ion module, the saturation of spins was able to resonate at a target frequency.¹⁷ However, the fixed fat-suppression bandwidth may not be sufficient to cope with B₀ inhomogeneities around the heart. Decreasing the bandwidth of the tip-down RF pulse attenuated off-resonance fat signals¹⁹ but depended on a precise RF-excitation angle, thus being sensitive to B₁ inhomogeneities while still requiring an additional fat-saturation module. Moreover, the increase in RF-excitation angle of the tip-down and tip-up pulse, required to negate inversion recovery of the fat signal in-between the T₂-Prep and the start of the acquisition, reduced the efficiency of the T₂ preparation of on-resonance water.¹⁹

The goal was to develop a novel T₂-Prep approach with a dephasing tip-down RF pulse that addresses the aforementioned challenges of robustness to B₀ and B₁ inhomogeneities while preserving T₂ contrast and simultaneously suppressing fat. The sensitivity of this technique to B₀ and B₁ inhomogeneities, as well as the effect of changing T₂-Prep durations and T₁ and T₂ relaxation times, was quantified by numerical simulations. The simulation results were validated in phantom and electrocardiogram (ECG)-triggered navigator-gated acquisitions of the human heart in healthy volunteers and were compared against routinely used techniques.

2 | METHODS

2.1 | Tip-down RF pulse design

The tip-down RF excitation pulse of an adiabatic T₂-Prep module¹⁶ was replaced by a custom-designed pulse (Figure 1A). The purpose of the RF design is to rotate both on- and off-resonance spins into the transverse plane while introducing a specific phase difference ($\Delta\varphi$) between the two spin populations at the T₂-Prep echo time (Figure 1B). Then, the nonselective tip-up pulse rotates the on-resonance magnetization back along the longitudinal axis, but because of the phase difference $\Delta\varphi$, the off-resonance spins are rotated into the transverse plane and spoiled by subsequent spoiler gradients (Figure 1C).

The proposed fat-suppressing phaser adiabatic T₂-preparation (PA-T₂-Prep) has a bandwidth that comprises both water and fat (Figure 1D), and $\Delta\varphi$ can be adjusted to obtain the desired longitudinal components of the off-resonance magnetization at the end of the module, without altering the T₂ preparation of on-resonance spins and without increasing the RF power. Fat magnetization is rotated with each applied RF pulse, which increases the robustness to B₁ inhomogeneities.

The RF profile of the tip-down pulse was approximated as the inverse Fourier transform of two rectangular functions representing the desired transverse magnetization of water and fat. One function represents the magnetization with frequencies below f_0 (fat) and bandwidth BW/2 that will be spoiled after T₂ preparation. The other represents the magnetization with frequencies above f_0 and bandwidth BW/2 that will be T₂ prepared (Figure 1D). In addition, a phase of $\pm\Delta\varphi/2$ is introduced to make the total phase difference $\Delta\varphi$ (Figure 1D). Following an inverse Fourier transform, the pulse shape is proportional to (Figure 1E):

$$\frac{1}{2} \text{sinc} \left(\frac{2\pi BW/2}{2\pi} t \right) \left(e^{i\frac{\Delta\varphi}{2}} e^{i2\pi t BW/4} + e^{-i\frac{\Delta\varphi}{2}} e^{-i2\pi t BW/4} \right) \quad (1)$$

$$= \text{sinc} \left(\frac{BW}{2} t \right) \cos \left(\pi \frac{BW}{2} t + \Delta\varphi/2 \right)$$

where sinc is the normalized cardinal sine function and t is time. The pulse duration PD was set to 8180 μs , the upper limit imposed by the vendor-provided source code. The pulse bandwidth was chosen to have a fat-suppression bandwidth close to 700 Hz (total bandwidth 1400 Hz) while having zero-crossings at the beginning and the end of the pulse, which is satisfied if $BW = \frac{2k}{PD}$, $k \in \mathbb{Z}^*$. BW was set to 1467 Hz (ie, $k = 3$), the RF-excitation angle was kept to 90°; the pulse off-resonance frequency (f_0) was set to -100 Hz, in-between water (0 Hz) and fat (-407 Hz). The optimal $\Delta\varphi$ for water-fat-phase separation, facilitating fat suppression, was initially determined using simulations and subsequently fine-tuned in a phantom. To compensate for phase gain based on f_0 and $\Delta\varphi$, the initial phase of the phaser tip-down pulse was set to $-\frac{1}{2} (PD2\pi f_0 + \Delta\varphi)$.

Although a small flip-angle approximation was used for the PA-T₂-Prep design, a comparison with Bloch simulations shows negligible impact (<5°) on the amplitude and phase of the magnetization (Supporting Information Figure S1).

2.2 | Numerical simulations

The effects of the conventional adiabatic T₂-prep (CA-T₂-Prep)¹⁶ with CHESS fat saturation (+FS) and the proposed PA-T₂-Prep on the longitudinal magnetization were quantified using numerical simulations performed in MATLAB (The MathWorks). The tip-down and tip-up RF pulses were modeled as Hamming-windowed sinc functions of 800 μs of opposite polarity for the CA-T₂-Prep+FS. For the

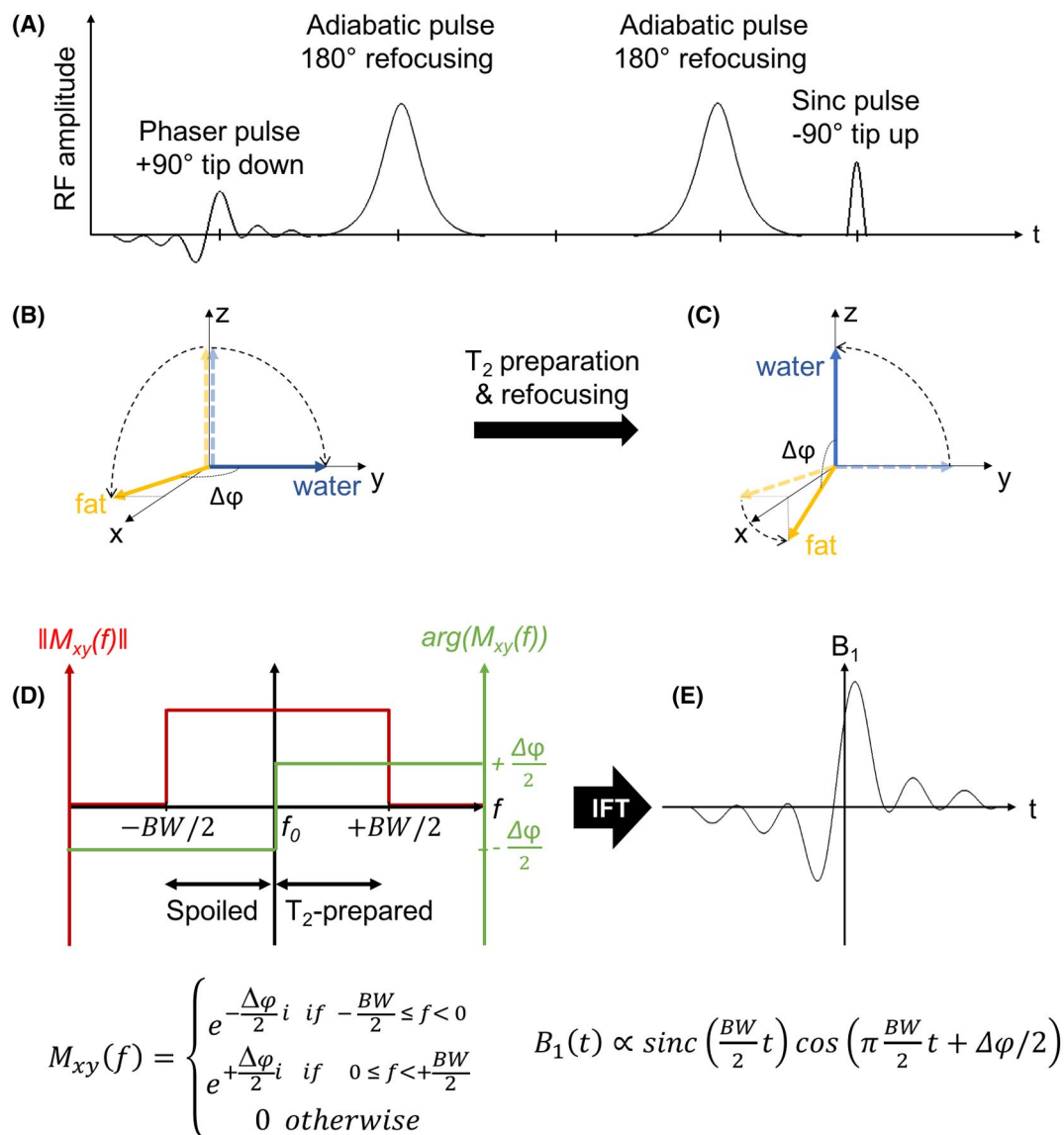


FIGURE 1 Diagram of the proposed phaser T_2 -preparation module and design of the phaser tip-down radiofrequency (RF) pulse. A, Overview of RF pulses used in the T_2 preparation module. The module is followed by a spoiling gradient (not illustrated). B, Excitation of the water (blue) and fat (yellow) magnetizations by the phaser tip-down pulse. The solid and dashed vectors represent the magnetization before and after the excitation, respectively, and the black-dashed trajectories represent their rotations. Both fat and water are rotated into the transverse plane, but the pulse introduces a phase difference $\Delta\phi$ between the two. C, Excitation of the water and fat magnetizations by broadband tip-up pulse. The T_2 -prepared–water magnetization is restored along the longitudinal axis whereas the fat is kept near the transverse plane because of $\Delta\phi$. D, Desired transverse magnetization fraction $\|M_{xy}(f)\|$ (red) and magnetization phase $\arg(M_{xy}(f))$ (green) after the phaser tip-down RF excitation as function of spin off-resonance frequency. BW: RF-excitation bandwidth, $\Delta\phi$: phase difference between fat and water magnetization, f_0 : RF-excitation–pulse frequency (E) B_1 amplitude of the phaser tip-down RF-excitation pulse as a function of time, calculated as the inverse Fourier transform of (D). A Bloch simulation of the RF-pulse profile (1E), as well as the small flip-angle approximation, can be found in Supporting Information Figure S1

PA- T_2 -Prep, the tip-down pulse as described above was used, whereas the tip-up pulse was identical to that of the CA- T_2 -Prep. The two hyperbolic secant refocusing adiabatic pulses were modeled using their RF-pulse shapes as implemented in the sequence with an excitation bandwidth of ± 800 Hz. The CHES pulse was modeled as implemented in the sequence, a $5120 \mu\text{s}$, -407 Hz Gaussian pulse with RF excitation angle = 100° . The simulations were performed by Euler integration

of the Bloch equations using steps of $1 \mu\text{s}$. The T_1 and T_2 relaxation times were set to those of fat at 200 ms and 50 ms, the off-resonance frequency was varied from -1000 Hz to 1000 Hz, and the B_1 amplitude ranged from 0% to 200% to account for B_0 and B_1 inhomogeneities. Magnetization was considered suppressed if its longitudinal component at the end of the T_2 -Prep was reduced to between $\pm 10\%$ of the starting magnetization M_0 . The excitation bandwidth reflects

the region of longitudinal magnetization being $\pm 10\%$ from the on-resonance magnetization at 100% B_1 amplitude. Note that 100% M_0 is not possible because of the T_2 -Prep module.

Additional simulations were performed to investigate the effect of different T_2 -Prep durations and $\Delta\phi$ on the longitudinal magnetization of blood ($T_1/T_2 = 1463/221$ ms), myocardium ($T_1/T_2 = 1072/31$ ms), and fat ($T_1/T_2 = 211/42$ ms) compartments with relaxation times determined in our “heart” phantom to enable a comparison with experimental data. A 6-peak fat model was used^{20,21} with frequency components of -469 Hz, -420 Hz, -321 Hz, -239 Hz, -48 Hz, and 74 Hz with respective amplitudes of 0.087 , 0.694 , 0.128 , 0.004 , 0.039 , and 0.048 .

2.3 | Phantom studies

A three-compartment cylindrical heart phantom was used that contains mixed solutions of agar and NiCl_2 (Sigma-Aldrich)²² or baby oil (Johnson & Johnson), mimicking the magnetic relaxation properties of blood ($T_1 = 1463 \pm 24$ ms, $T_2 = 221 \pm 15$ ms), muscle ($T_1 = 1072 \pm 8$ ms, $T_2 = 31 \pm 0.4$ ms), and fat ($T_1 = 211 \pm 1$ ms, $T_2 = 42 \pm 0.3$ ms). Acquisitions were performed on a clinical 3T scanner (MAGNETOM Prisma^{fit}; Siemens Healthcare) using an 18-channel spine and 16-channel chest RF coil with a segmented three-dimensional Cartesian gradient echo sequence with a field of view of $160 \times 96 \times 95$ mm³ and resolution of $1 \times 1 \times 5$ mm³. After the T_2 -Prep with 10-ms hyperbolic secant adiabatic refocusing pulses,^{5,15} 25 k-space lines were acquired using centric ordering: pulse repetition time = 5 ms, echo time = 2.5 ms, RF excitation angle = 15° , bandwidth = 501 Hz/pixel, and time between T_2 -Preps = 1 s. The T_2 -Prep duration was varied from 40 ms to 60 ms to 80 ms and the $\Delta\phi$ was varied between 90° and 270° by steps of 5° (randomized acquisition order), and the resulting average signal from each of the three compartments was quantified. The $\Delta\phi$ yielding the lowest fat signal for a T_2 -Prep duration of 40 ms was used for the rest of the study.

Additional experiments were performed in a National Institute of Standards and Technology phantom to investigate the effect of a range of T_1 and T_2 values, T_2 -Prep durations, and $\Delta\phi$ values on the signal behavior in each compartment.

Mean compartment signals were quantified after using five different T_2 -Prep modules: no T_2 -Prep, CA- T_2 -Prep, CA- T_2 -Prep+FS, PA- T_2 -Prep, and the water-selective adiabatic T_2 -Prep with fat saturation (WSA- T_2 -Prep+FS).¹⁹ The RF-excitation angle of the CHESS pulse was set to 100° , which was chosen based on experimental fine-tuning performed in the heart phantom. The B_0 and B_1 fields were intentionally not shimmed to test the sensitivity of each technique to inhomogeneities. Scan-rescan acquisitions were performed for quantification of blood, myocardium, and fat-compartment

mean signal and noise using the acquisition-subtraction method.²³ A 1-h-long scan with 100 averages was acquired prior to the scan-rescan experiment to reach thermal steady state for true noise quantification. A compartment-specific SNR was computed relative to the no T_2 -Prep case to emphasize compartment-specific differences across T_2 -Preps. A B_0 map with a ± 1000 Hz bandwidth was computed from two acquisitions with the same acquisition parameters as described previously, without T_2 -Prep and with an echo time of 2.5 ms and 3.0 ms. Scaling in B_0 maps was cropped to ± 500 Hz. Additionally, a B_1 map from two acquisitions with RF-excitation angles of 60° and 120° was computed using a double-angle method²⁴ and a pulse-repetition time of 10 s.

2.4 | In vivo study

Human studies were approved by the local ethics committee. Whole-heart free-breathing ECG-triggered navigator-gated scans were acquired in healthy volunteers who gave written and informed consent ($N = 6$, age = 27 ± 4 years). To keep the scan time below 1 h per participant, only the CA- T_2 -Prep, CA- T_2 -Prep+FS, and PA- T_2 -Prep were tested. The same imaging sequence was used as described earlier, except for a field of view of $230 \times 368 \times 86.4$ mm³ and an isotropic pixel size of 1.2 mm. Images were reformatted using Soap-Bubble, a semiautomated reformatting and vessel-tracking software package.²⁵ The right coronary artery (RCA) vessel sharpness was computed in a 4-cm segment using Soap-Bubble. Blood, myocardium, chest fat, and epicardial SNR were quantified in chest fat, epicardial fat, blood, and myocardium. The SNR was approximated by dividing the average signal from regions of interests drawn in respective tissues by the standard deviation of the background noise. The CNR was quantified between blood and myocardium compartments, as well as blood and epicardial fat and myocardium and epicardial fat. Differences between the CA- T_2 -Prep and PA- T_2 -Prep, as well as between the CA- T_2 -Prep+FS and PA- T_2 -Prep, were tested via a Student's t test for paired data. A Bonferroni correction was applied to correct for multiple comparisons: P values obtained with individual t tests were multiplied with the amount of comparisons to keep the significance threshold at $P < .05$. Additionally, the specific absorption rate (SAR) was recorded from the system console.

3 | RESULTS

3.1 | Numerical simulation

The PA- T_2 -Prep simulation (Figure 2A) predicted an increased robustness in fat suppression against B_0 and B_1 field inhomogeneities in comparison with the CA- T_2 -Prep+FS

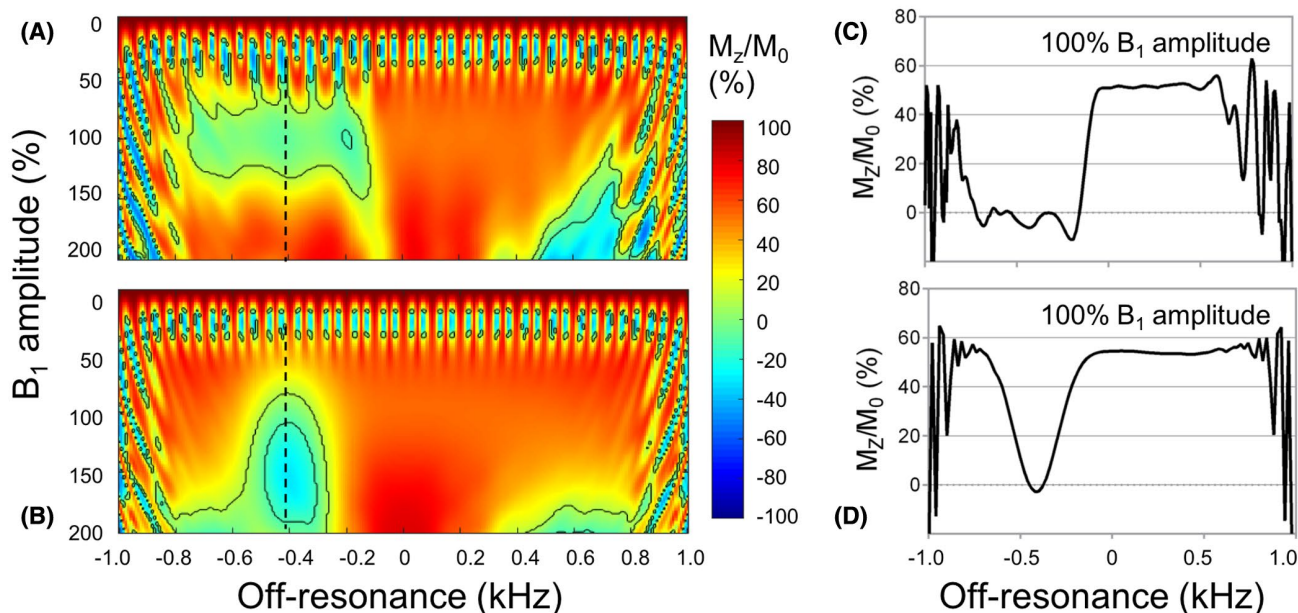


FIGURE 2 Numerical simulation of the performance of the entire phaser adiabatic T_2 -Prep (PA- T_2 -Prep) and the conventional adiabatic T_2 -Prep with fat saturation (CA- T_2 -Prep+FS). The longitudinal magnetization (M_z) as a fraction of the initial magnetization (M_0) is plotted as a function of B_1 strength and off-resonance frequency after application of (A) the PA- T_2 -Prep and (B) CA- T_2 -Prep+FS. A B_1 value of 100% corresponds to the desired applied RF amplitude. The dashed line indicates the center frequency of fat (-407 Hz), and the outlined green regions correspond to a resulting longitudinal magnetization with a magnitude less than 10% of the initial magnetization. The excitation bandwidth of the adiabatic hyperbolic secant pulse that ranges from -800 to 800 Hz can be clearly observed. Line plots of signal behavior versus off-resonance frequency at 100% B_1 amplitude for both (C) PA- T_2 -Prep and (D) CA- T_2 -Prep+FS

(Figure 2B). For an off-resonance frequency of -407 Hz, the magnetization was suppressed if B_1 was between 84% and 111% for the CA- T_2 -Prep+FS versus 75% and 130% for the PA- T_2 -Prep. At a B_1 amplitude of 100%, the fat-suppression bandwidth was 162 Hz for the CA- T_2 -Prep+FS and 627 Hz for the PA- T_2 -Prep (Figure 2C,D). At 100% B_1 amplitude the on-resonance magnetization was approximately 54% and approximately 51% for the CA- T_2 -Prep+FS and PA- T_2 -Prep, respectively (Figure 2C,D). On-resonance magnetization was excited if B_1 was between 60% and 125% the CA- T_2 -Prep+FS versus 67% and 127% for the PA- T_2 -Prep. At a B_1 amplitude of 100%, the excitation bandwidth was between -140 Hz and 775 Hz for the CA- T_2 -Prep+FS and between -66 Hz and 601 Hz for the PA- T_2 -Prep.

As expected based on our pulse design, simulation results show that the choice of $\Delta\phi$ affects the level of fat suppression (Figure 3A), whereas it does not affect the on-resonance signal. The optimal $\Delta\phi$ is affected by the T_2 -Prep duration and varied from 105° to 135° . However, once the optimal $\Delta\phi$ for a given T_2 -Prep duration (d_1) is found, the optimal $\Delta\phi$ for another T_2 -Prep duration (d_2) can be estimated as follows (derivation in Supporting Information):

$$\Delta\phi_2 = \sin^{-1} \left(e^{-\frac{d_2-d_1}{T_2}} * \sin \left(\Delta\phi_1 - \frac{\pi}{2} \right) \right) + \frac{\pi}{2} \quad (2)$$

3.2 | Phantom studies

The minimum average fat signal occurred at $\Delta\phi$, ranging from 105° to 135° , depending on the T_2 -Prep duration (Figure 3B). The choice of $\Delta\phi$ only affects the level of fat suppression (Figure 3B), and it does not affect the on-resonance signal nor is it influenced by changes in T_1 or T_2 (Figure 3C-H).

The SNR of the blood, myocardium, and fat compartment using either the CA- T_2 -Prep, CA- T_2 -Prep+FS, WSA- T_2 -Prep+FS, and PA- T_2 -Prep relative to using no T_2 -Prep show differences in fat suppression and T_2 -weighting (Figure 4). Compared with the CA- T_2 -Prep, CA- T_2 -Prep+FS and WSA- T_2 -Prep+FS, the PA- T_2 -Prep reduced the lipid signal by 93.2%, 70.0%, and 66.1%, respectively. The blood and myocardium compartment SNR in PA- T_2 -Prep images were, respectively, 0.7% and 0.9% lower than in the CA- T_2 -Prep, 0.1% and 3.8% lower than in the CA- T_2 -Prep+FS, and 3.4% and 26.9% lower than in the WSA- T_2 -Prep+FS (Figure 4). Compared with the CA- T_2 -Prep, CA- T_2 -Prep+FS and WSA- T_2 -Prep+FS, the PA- T_2 -Prep increased blood-myocardium CNR by -0.5% , 3.4% , and 35.3% , the blood-fat CNR by -1399% , 22.5% , and 13.1% , and the myocardium-fat CNR by -166% , 62.3% , and -7.2% (Figure 4).

Fat suppression using the PA- T_2 -Prep was improved in regions where field inhomogeneities hindered the capabilities of other methods (Figure 4, orange arrows). In contrast to the

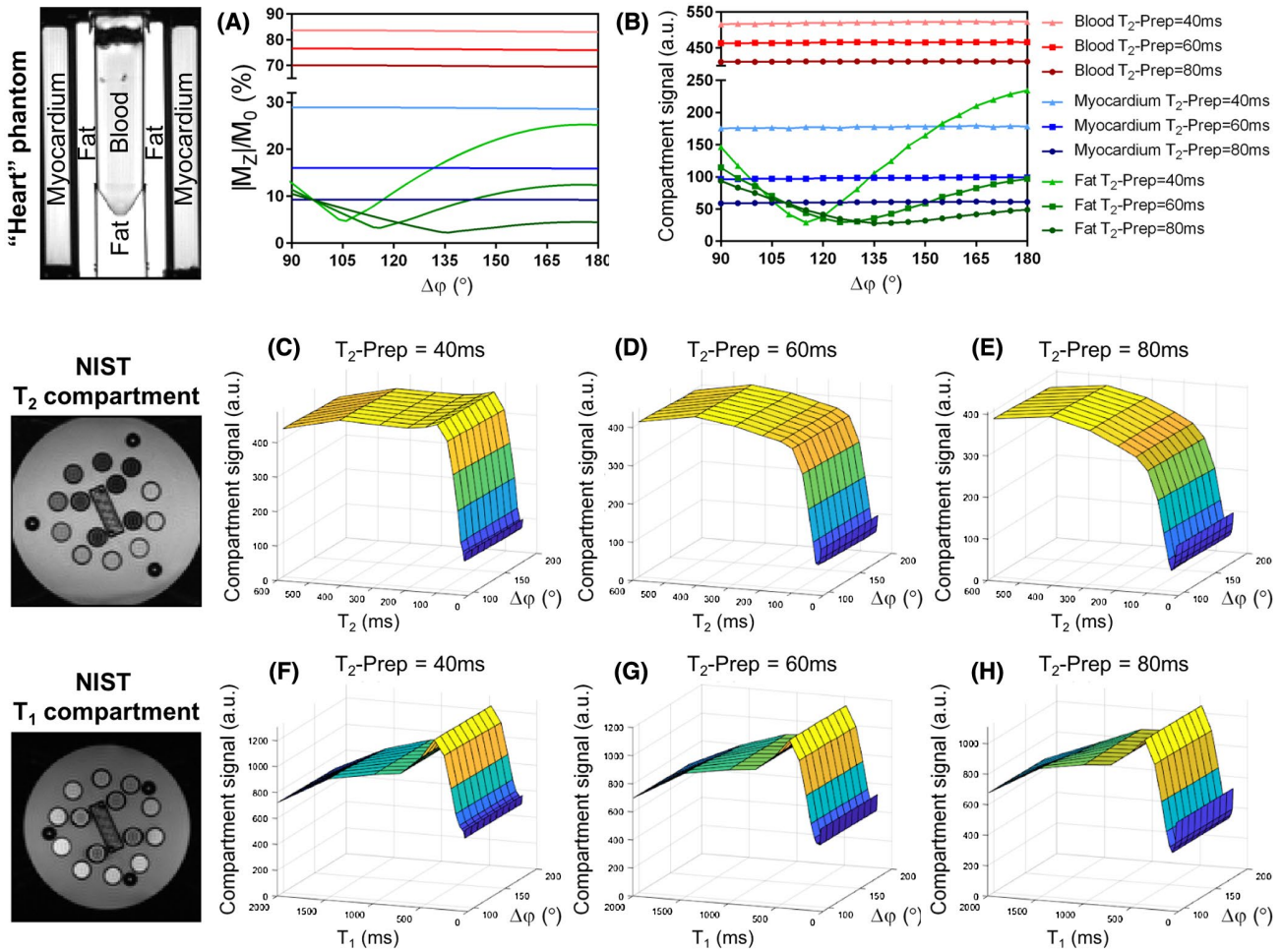


FIGURE 3 A, Simulated magnetization from blood, myocardium, and fat compartments with relaxation times identical to the “heart” phantom. Local minima on the fat signal curve indicate optimal fat suppression ranging from $\Delta\phi = 106^\circ$ to $\Delta\phi = 136^\circ$, depending on the T_2 -Prep duration. B, Signal-to-noise ratio (SNR) of the blood, myocardium, and fat compartments determined from experiments in the heart phantom show an optimal $\Delta\phi$ ranging from 115° to 135° , depending on the T_2 -Prep duration. SNR of different T_2 compartments (C,D,E) and T_1 compartments (F,G,H) in a National Institute of Standards and Technology (NIST) phantom show the expected effect of changes in T_2 -Prep durations but no effects of changing $\Delta\phi$. Both simulations and experiments show that on-resonance compartments are unaffected by the change of $\Delta\phi$

CA- T_2 -Prep+FS and PA- T_2 -Prep, the WSA- T_2 -Prep reduced blood and myocardium signals in regions where the B_0 imperfections increased the precession frequency by more than 200 Hz (Figure 4, green arrows).

3.3 | In vivo study

The PA- T_2 -Prep visually increased the RCA vessel conspicuity compared with the CA- T_2 -Prep+FS and the CA- T_2 -Prep (Figure 5A). The PA- T_2 -Prep reduced chest fat SNR to 7.2 ± 1.9 from 34 ± 10.8 (CA- T_2 -Prep, $P < .005$) and 15.3 ± 5.2 (CA- T_2 -Prep+FS, $P < .05$; Figure 5B). Epicardial fat SNR was reduced to 2.5 ± 0.8 (PA- T_2 -Prep, $P < .005$) to 10 ± 2.5 (CA- T_2 -Prep, $P < .05$) and 4.6 ± 1.9 (CA- T_2 -Prep+FS, $P < .05$; Figure 5B). No significant differences between blood SNR and myocardium SNR was observed across the three different T_2 -Prep approaches (Figure 5B), similar for

the CNR between blood and myocardium (Figure 5C). The PA- T_2 -Prep results reported the highest CNR between blood and epicardial fat, as well as between myocardium and epicardial fat (Figure 5C). Using the PA- T_2 -Prep approach the RCA vessel sharpness was $40.2 + 9.6\%$, compared with $21.0 + 6.4\%$ (CA- T_2 -Prep, $P < .005$) and $33.6 + 6.4\%$ (CA- T_2 -Prep+FS, $P = .08$; Figure 5D). The SAR increased by 1% using the PA- T_2 -Prep compared with the two other methods.

4 | DISCUSSION

As shown by the Bloch equation simulations, the PA- T_2 -Prep not only increases the fat saturation bandwidth, but also avoids water signal attenuation when its resonance frequency is shifted caused by field inhomogeneities. Additionally, the multiple rotations of the fat magnetization during the PA- T_2 -Prep decrease the fat suppression

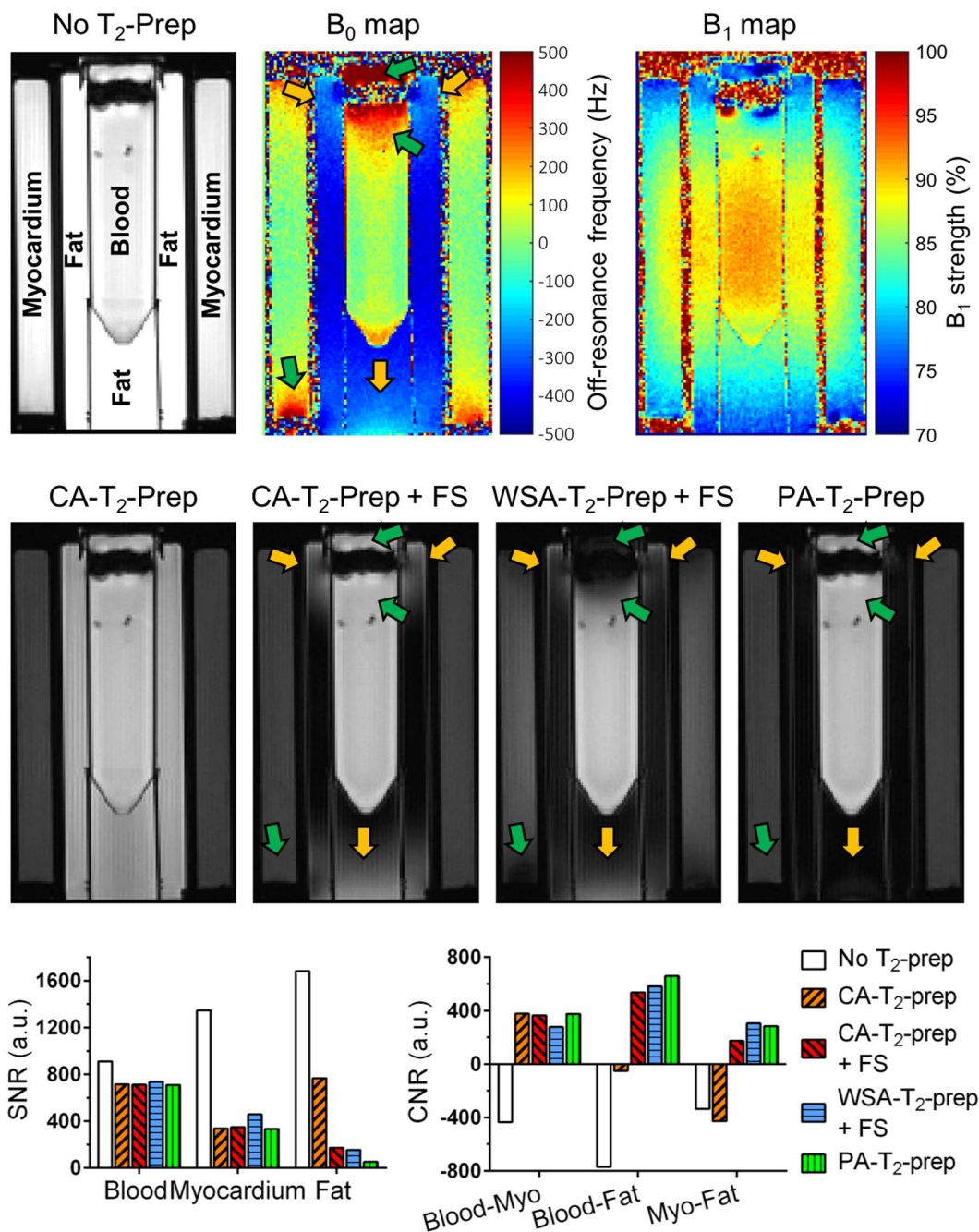


FIGURE 4 A comparison of the different T_2 -preparation (T_2 -Prep) methods in the multicompartiment “heart” phantom with corresponding B_0 and B_1 maps. Images acquired with no T_2 -Prep, the conventional adiabatic T_2 -Prep (CA- T_2 -Prep) without and with fat saturation (FS), the water-selective adiabatic T_2 -Prep (WSA- T_2 -Prep) and the phaser adiabatic T_2 -Prep (PA- T_2 -Prep). Orange arrows indicate locations of improved fat suppression using the PA- T_2 -Prep compared with other fat-suppression methods. Green arrows indicate positive off-resonance regions in which the water-selective method attenuated the signal that was not observed using the PA- T_2 -Prep. The signal-to-noise ratio (SNR) and contrast-to-noise ratio (bottom panels) were computed for each technique. The blood and myocardium signals in the CA- T_2 -Prep, CA- T_2 -Prep+FS, and PA- T_2 -Prep were similar. However, the 120° radiofrequency-excitation angle of WSA- T_2 -Prep reduced the efficiency of the T_2 preparation, resulting in increased myocardium SNR. The fat signal was most reduced using the PA- T_2 -Prep

dependence on B_1 precision compared with the use of a single fat saturation pulse.

The WSA- T_2 -Prep¹⁹ achieved fat suppression by increasing the RF excitation angle of tip-down and tip-up pulses, which affects on-resonance magnetization and results in a loss

of T_2 preparation. In comparison, the PA- T_2 -Prep rotates the magnetization 90° such that the effectiveness of the T_2 preparation is conserved, as confirmed by the measured SNR in the phantom and in vivo experiments. The water-fat-phase separation $\Delta\phi$ influences the orientation of the fat magnetization

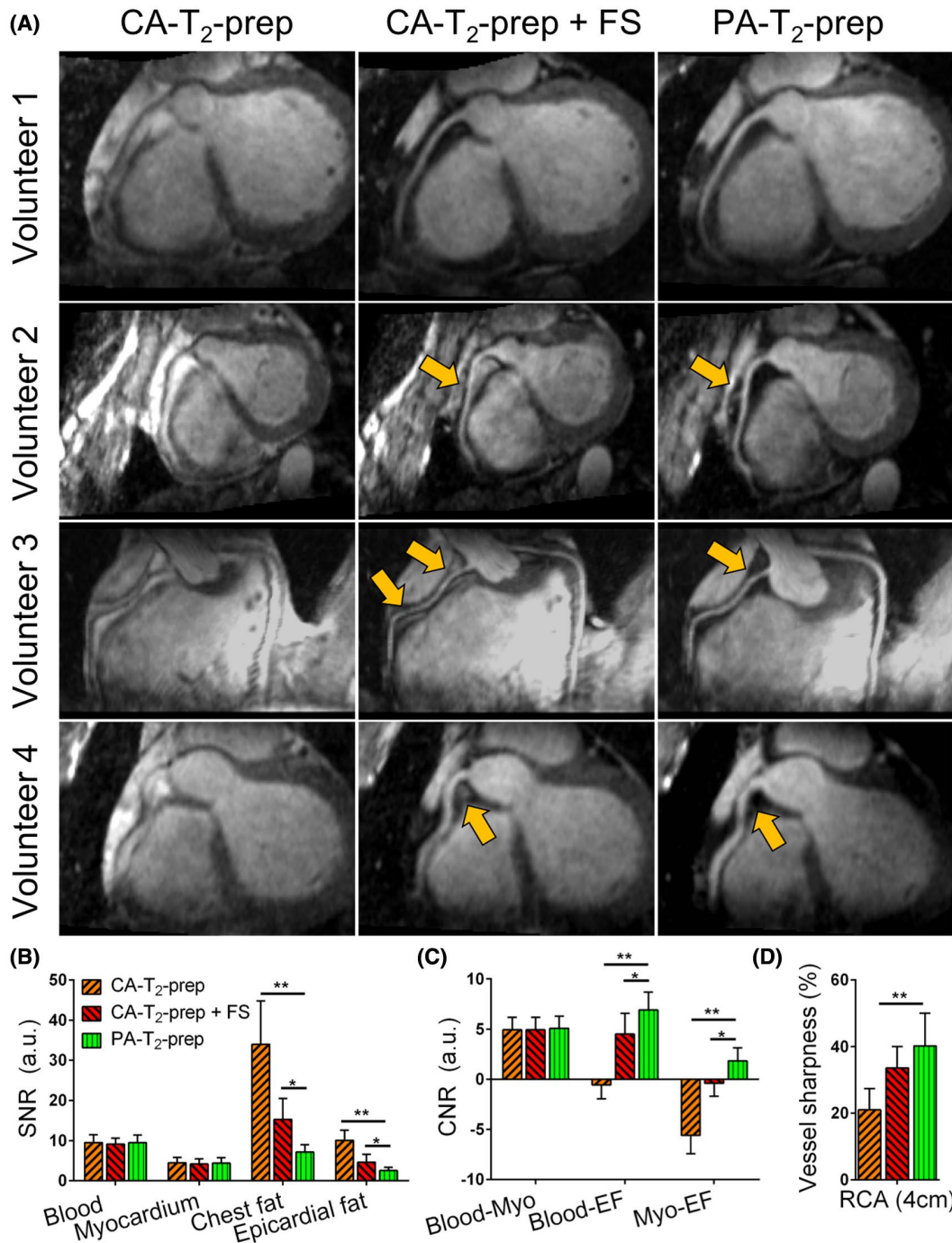


FIGURE 5 A comparison of the T₂-preparation (T₂-Prep) modules in the human heart in vivo at 3T. A, Electrocardiogram-triggered navigator-gated reformatted images of healthy volunteers using the conventional adiabatic T₂-Prep without (CA-T₂-Prep) and with fat saturation (CA-T₂-Prep+FS) and the phaser adiabatic T₂-Prep (PA-T₂-Prep). Orange arrows indicate improved fat suppression using the PA-T₂-Prep compared with the conventional fat suppression (FS) using chemically selective saturation. B, Signal-to-noise ratio. C, Contrast-to-noise ratio. D, Vessel sharpness. **P* < .05, ***P* < .005

after the T₂-Prep (Figure 1) and can be adjusted to adapt the module to different pulse sequences. For example, a balanced steady-state free-precession acquisition may require ramp-up pulses between the T₂-Prep and the acquisition during which the fat signal may recover. In this case, Δφ may be increased to compensate for this additional recovery.

Similar to the CA-T₂-Prep+FS, the WSA-T₂-Prep, or a CHESS fat-saturation pulse, the PA-T₂-Prep suppresses the fat once before the acquisition. After suppression, the fat magnetization will start to recover; consequentially, the effectiveness of the fat suppression is limited by the pulse sequence that follows. Although simulations provided a good initial estimate

of the optimal $\Delta\phi$, within an imaging sequence there are many parameters that affect the final signal weighting of fat. It is complex to simulate accurately; hence, there are small discrepancies in optimal $\Delta\phi$ between simulations and experiments and the need for an experimental fine-tuning. Once $\Delta\phi$ is found it, can be transferred to the in vivo setting provided that the same acquisition parameters are used, and that the phantom adequately represents the fat tissue of interest. Otherwise, an experimental fine-tuning of $\Delta\phi$ is required in vivo. In sequences using Cartesian sampling trajectories, the PA- T_2 -Prep may remove the need for additional fat-suppression modules and thus reduce SAR. However, it will be less suitable for acquisition schemes that do not allow for centric reordering of the phase-encoding planes of k-space, such as radial acquisitions. Although water-selective excitation approaches may be more suitable for fat suppression in radial whole-heart MRI at 3T,²⁶⁻²⁹ acquisitions requiring T_2 -Prep modules may still benefit from the proposed approach because it offers an additional, tuneable range of fat suppression. Recently, T_2 -Prep approaches designed for coronary artery imaging at 1.5T included outer volume-suppression strategies,^{30,31} with integrated spectral spatial sinc pulses for fat suppression.³² Their utility at 3T remains to be investigated, considering SAR may be higher and balanced steady-state free-precession less performant at higher field strengths; therefore, these methods were not compared in the current study. Another limitation includes the minimum duration of the PA- T_2 -Prep module that the lengthy tip-down pulse imposes. The PA- T_2 -Prep requires at least 29 ms compared with 21.7 ms for the CA- T_2 -Prep, which may limit the range of available T_2 contrast, although this may be addressed using a shorter adiabatic refocusing pulse pair. It should be noted that the glycerol and olefinic fat resonances at 5.3 and 4.2 ppm fall within the excitation band of the PA- T_2 -Prep and would not be suppressed, which is also the case with the aforementioned existing approaches and would not be suppressed. Because these resonances constitute approximately 9% of the fat signal, this is not considered a significant disadvantage.

The proposed PA- T_2 -Prep has a narrow excitation bandwidth that may result in on-resonance water being suppressed when B_0 conditions are not optimal. In the phantom experiments, a slight decrease of <1% (yet above the noise level) in blood and myocardium compartment signal was observed. Besides the narrow excitation bandwidth, this slight loss could also be explained by the excitation profile ripples of the phaser tip-down pulse caused by its finite duration. Nevertheless, strong effects of diminished on-resonance excitation were not observed.

A translation of the PA- T_2 -Prep to different field strengths is possible; higher magnetic field strengths would require a decrease in the duration of the tip-down RF excitation pulse, and lower magnetic field strengths would require an

increase. Furthermore, the principle of our PA- T_2 -Prep design could be translated to any magnetization preparation module. Calibrations would need to be performed to find the optimal $\Delta\phi$, but there are no theoretical barriers. For example, in T_2 -mapping techniques that use incrementing T_2 -Prep durations, it may reduce chemical shift artifacts that hinder cartilage delineation and quantification,⁷ and may obviate the use of additional fat-suppression modules.^{4,5,33} It could also be integrated with T_1 - and T_2 -mapping techniques.^{34,35} The approach may be extended to applications that use T_2 -Prep modules combined with inversion recovery,^{36,37} as well as modules for motion-sensitized driven-equilibrium^{38,39} for blood signal suppression.

5 | CONCLUSION

In this study, a novel T_2 -Prep approach was developed that provides a large spectral bandwidth of fat suppression. The technique is robust against B_0 and B_1 inhomogeneities, and preserves blood-myocardium SNR and CNR. As a result, the RCA vessel sharpness was increased compared with conventional approaches.


ACKNOWLEDGMENTS

Jessica A. M. Bastiaansen received funding from the Swiss National Science Foundation (grant nos. PZ00P3_167871 and PCEFP2_194296), the Emma Muschamp Foundation, the Swiss Heart Foundation (grant nos. FF18054 and FF20136), and the Bourse Pro Femmes from the University of Lausanne. Ruud B. van Heeswijk received funding from the Swiss National Science Foundation (grant no. 32003B_182615) and Matthias Stuber from the Swiss National Science Foundation (grant nos. 320030_173129 and 326030_150828).

DATA AVAILABILITY STATEMENT

All data and code are available upon request.

ORCID

Ruud B. van Heeswijk  <https://orcid.org/0000-0001-5028-4521>

[org/0000-0001-5028-4521](https://orcid.org/0000-0001-5028-4521)

Matthias Stuber  <https://orcid.org/0000-0001-9843-2028>

Jessica A. M. Bastiaansen  <https://orcid.org/0000-0002-5485-1308>

[org/0000-0002-5485-1308](https://orcid.org/0000-0002-5485-1308)

TWITTER

Jessica A. M. Bastiaansen  @jessica_b_

REFERENCES

1. Brittain JH, Hu BS, Wright GA, Meyer CH, Macovski A, Nishimura DG. Coronary angiography with magnetization-prepared T2 contrast. *Magn Reson Med*. 1995;33:689-696.

2. Shea SM, Deshpande VS, Chung Y-C, Li D. Three-dimensional true-FISP imaging of the coronary arteries: improved contrast with T2-preparation. *J Magn Reson Imaging*. 2002;15:597-602.
3. Botnar RM, Stuber M, Dianas PG, Kissinger KV, Manning WJ. Improved coronary artery definition with T2-weighted, free-breathing, three-dimensional coronary MRA. *Circulation*. 1999;99:3139-3148.
4. Foltz WD, Al-Kwafi O, Sussman MS, Stainsby JA, Wright GA. Optimized spiral imaging for measurement of myocardial T2 relaxation. *Magn Reson Med*. 2003;49:1089-1097.
5. van Heeswijk RB, Feliciano H, Bongard C, et al. Free-breathing 3 T magnetic resonance T2-mapping of the heart. *JACC Cardiovasc Imaging*. 2012;5:1231-1239.
6. Colotti R, Omoumi P, Bonanno G, Ledoux J-B, van Heeswijk RB. Isotropic three-dimensional T2 mapping of knee cartilage: development and validation. *J Magn Reson Imaging*. 2018;47:362-371.
7. Colotti R, Omoumi P, van Heeswijk RB, Bastiaansen JAM. Simultaneous fat-free isotropic 3D anatomical imaging and T2 mapping of knee cartilage with lipid-insensitive binomial off-resonant RF excitation (LIBRE) pulses. *J Magn Reson Imaging*. 2019;49:1275-1284.
8. Manning WJ, Li W, Boyle NG, Edelman RR. Fat-suppressed breath-hold magnetic resonance coronary angiography. *Circulation*. 1993;87:94-104.
9. Haase A, Frahm J, Hanicke W, Matthaei D. H-1-NMR chemical-shift selective (Chess) imaging. *Phys Med Biol*. 1985;30:341-344.
10. Meyer CH, Pauly JM, Macovski A, Nishimura DG. Simultaneous spatial and spectral selective excitation. *Magn Reson Med*. 1990;15:287-304.
11. Schick F. Simultaneous highly selective MR water and fat imaging using a simple new type of spectral-spatial excitation. *Magn Reson Med*. 1998;40:194-202.
12. Bastiaansen JAM, Stuber M. Flexible water excitation for fat-free MRI at 3T using lipid insensitive binomial off-resonant RF excitation (LIBRE) pulses. *Magn Reson Med*. 2018;79:3007-3017.
13. van Elderen SGC, Versluis MJ, Westenberg JJM, et al. Right coronary MR angiography at 7 T: a direct quantitative and qualitative comparison with 3 T in young healthy volunteers. *Radiology*. 2010;257:254-259.
14. Bhat H, Yang Q, Zuehlsdorff S, Li K, Li D. Contrast-enhanced whole-heart coronary MRA at 3T using interleaved EPI. *Invest Radiol*. 2010;45:458-464.
15. Hwang TL, van Zijl PC, Garwood M. Fast broadband inversion by adiabatic pulses. *J Magn Reson*. 1998;133:200-203.
16. Nezafat R, Stuber M, Ouwerkerk R, Gharib AM, Desai MY, Pettigrew RI. B1-insensitive T2 preparation for improved coronary magnetic resonance angiography at 3 T. *Magn Reson Med*. 2006;55:858-864.
17. Nezafat R, Ouwerkerk R, Derbyshire AJ, Stuber M, McVeigh ER. Spectrally selective B1-insensitive T2 magnetization preparation sequence. *Magn Reson Med*. 2009;61:1326-1335.
18. Soleimanifard S, Schär M, Hays AG, Prince JL, Weiss RG, Stuber M. A spatially-selective Implementation of the adiabatic T2Prep sequence for magnetic resonance angiography of the coronary arteries. *Magn Reson Med*. 2013;70:97-105.
19. Coristine AJ, van Heeswijk RB, Stuber M. Fat signal suppression for coronary MRA at 3T using a water-selective adiabatic T2 -preparation technique. *Magn Reson Med*. 2014;72:763-769.
20. Hamilton G, Yokoo T, Bydder M, et al. In vivo characterization of the liver fat 1H MR spectrum. *NMR Biomed*. 2011;24:784-790.
21. Wang X, Hernando D, Reeder SB. Sensitivity of chemical shift-encoded fat quantification to calibration of fat MR spectrum. *Magn Reson Med*. 2016;75:845-851.
22. Kraft KA, Fatouros PP, Clarke GD, Kishore PR. An MRI phantom material for quantitative relaxometry. *Magn Reson Med*. 1987;5:555-562.
23. Firbank MJ, Coulthard A, Harrison RM, Williams ED. A comparison of two methods for measuring the signal to noise ratio on MR images. *Phys Med Biol*. 1999;44:N261-N264.
24. Cunningham CH, Pauly JM, Nayak KS. Saturated double-angle method for rapid B1+ mapping. *Magn Reson Med*. 2006;55:1326-1333.
25. Etienne A, Botnar RM, Van Muiswinkel AM, Boesiger P, Manning WJ, Stuber M. "Soap-Bubble" visualization and quantitative analysis of 3D coronary magnetic resonance angiograms. *Magn Reson Med*. 2002;48:658-666.
26. Pang J, Sharif B, Fan Z, et al. ECG and navigator-free four-dimensional whole-heart coronary MRA for simultaneous visualization of cardiac anatomy and function. *Magn Reson Med*. 2014;72:1208-1217.
27. Bastiaansen JAM, van Heeswijk RB, Stuber M, Piccini D. Noncontrast free-breathing respiratory self-navigated coronary artery cardiovascular magnetic resonance angiography at 3 T using lipid insensitive binomial off-resonant excitation (LIBRE). *J Cardiovasc Magn Reson*. 2019;21:38.
28. Bastiaansen JAM, Piccini D, Sopra LD, et al. Natively fat-suppressed 5D whole-heart MRI with a radial free-running fast-interrupted steady-state (FISS) sequence at 1.5T and 3T. *Magn Reson Med*. 2020;83:45-55.
29. Masala N, Bastiaansen JAM, Sopra LD, et al. Free-running 5D coronary MR angiography at 1.5T using LIBRE water excitation pulses. *Magn Reson Med*. 2020;84:1470-1485.
30. Coristine AJ, van Heeswijk RB, Stuber M. Combined T2-preparation and two-dimensional pencil-beam inner volume selection. *Magn Reson Med*. 2015;74:529-536.
31. Luo J, Addy NO, Ingle RR, et al. Combined outer volume suppression and T2 preparation sequence for coronary angiography. *Magn Reson Med*. 2015;74:1632-1639.
32. Zeng DY, Baron CA, Malavé MO, et al. Combined T2-preparation and multidimensional outer volume suppression for coronary artery imaging with 3D cones trajectories. *Magn Reson Med*. 2020;83:2221-2231.
33. Giri S, Chung Y-C, Merchant A, et al. T2 quantification for improved detection of myocardial edema. *J Cardiovasc Magn Reson*. 2009;11:56.
34. Kvernby S, Warntjes MJB, Haraldsson H, Carlhäll C-J, Engvall J, Ebbers T. Simultaneous three-dimensional myocardial T1 and T2 mapping in one breath hold with 3D-QALAS. *J Cardiovasc Magn Reson*. 2014;16:102.
35. Hamilton JI, Jiang Y, Chen Y, et al. MR fingerprinting for rapid quantification of myocardial T1, T2, and proton spin density. *Magn Reson Med*. 2017;77:1446-1458.
36. Liu C-Y, Wieben O, Brittain JH, Reeder SB. Improved delayed enhanced myocardial imaging with T2-Prep inversion recovery magnetization preparation. *J Magn Reson Imaging*. 2008;28:1280-1286.
37. Liu C-Y, Bley TA, Wieben O, Brittain JH, Reeder SB. Flow-independent T2-prepared inversion recovery black-blood MR imaging. *J Magn Reson Imaging*. 2010;31:248-254.
38. Koktzoglou I, Li D. Diffusion-prepared segmented steady-state free precession: application to 3D black-blood cardiovascular

- magnetic resonance of the thoracic aorta and carotid artery walls. *J Cardiovasc Magn Reson.* 2007;9:33-42.
39. Wang J, Yarnykh VL, Hatsukami T, Chu B, Balu N, Yuan C. Improved suppression of plaque-mimicking artifacts in black-blood carotid atherosclerosis imaging using a multislice motion-sensitized driven-equilibrium (MSDE) turbo spin-echo (TSE) sequence. *Magn Reson Med.* 2007;58:973-981.

SUPPORTING INFORMATION

Additional Supporting Information may be found online in the Supporting Information section.

FIGURE S1 A comparison of the small flip angle approximation (left) and a Bloch simulation (right) of the RF pulse profile (Figure 1E). The difference between these two predictions are due to the violation of the assumption

of small flip angle. Within the excitation bandwidth (± 700 Hz), the ripples of the magnetization phase have an amplitude of approximately $\pm 5^\circ$, but the effect of these might not be visible in practice since they are averaged out across the wide frequency range of fat. The phase behavior outside the excitation bandwidth can be neglected since the amplitude of the transversal magnetization is negligible

How to cite this article: Arn L, van Heeswijk RB, Stuber M, Bastiaansen JAM. A robust broadband fat-suppressing phaser T_2 -preparation module for cardiac magnetic resonance imaging at 3T. *Magn Reson Med.* 2021;00:1–11. <https://doi.org/10.1002/mrm.28785>